

Structural diagrams and thermodynamics relating to temperature and compositions of $\text{Ag}_{561-n}\text{Cu}_n$ ($n = 0-561$) nanoalloys during cooling from atomic simulations

Yuanjiang Zhang^{1,#}, Mingyuan Che^{1,#}, Lin Zhang^{1,2,a}

¹Key Laboratory for Anisotropy and Texture of Materials (Ministry of Education), Northeastern University, Shenyang, 110819, China

²School of Materials Science and Engineering, Northeastern University, Shenyang, 110819, China

^azhanglin@imp.neu.edu.cn

[#]These authors contributed equally to this work and should be considered co-first authors.

Abstract: The packing changes of $\text{Ag}_{561-n}\text{Cu}_n$ ($n = 0-561$) nanoparticles during cooling were studied by molecular dynamics simulations at atomic scale. Structural diagrams as well as packing images presented liquid, disordered, and some ordered patterns. Pair distribution functions were used to characterize some typical structures. Potential energy and shape factors identified the transition's temperature regime and the effect of cooling on the shape's changes of the alloyed particles. The simulation results show composition effect on the transition temperatures and complex structural patterns. For these Cu-Ag nanoalloys, which contain small amount of Cu or Ag atoms, they show alternating FCC and icosahedral packing patterns at low temperatures, and core-shell configurations prefer to occur in the Cu-rich particles, where the Cu occupy the interior of the particles. Compositions and degree of orderliness in packing contribute to the entropy of the alloyed nanoparticles.

Keywords: nanoalloys; molecular dynamics; entropy; atomic simulations

1. Introduction

During recent decades, nano-alloy particles have received intensive attention from scientific researchers for their wide applications in quantum computers, chemical sensors, magnetic storage, nano-coatings and biomedicine due to their excellent properties in light, electricity, heat and magnetism^[1-6]. With the improvements of newly developed controllable capabilities in atomic precision, there has been a great progress in the study of alloyed nanoparticles, which show great diversities of atomic packing patterns and particle shapes, as well as significant differences in their physicochemical properties. Among them, binary nanoalloys play an important role in the fields of biomonitoring, fuel cells and optics, et al.^[7-13]. Ag can be used conductivity, and its nanoparticles have excellent optoelectronic, antioxidant and catalytic properties^[14-16]. Nevertheless, the high cost limits its applications. Substituting other metal elements in the particles is an important way to solve the problem^[17]. Cu has the similar $d^{10}s^1$ valences with those of Ag, which can be also used in oxidation, reduction, dehydrogenation, and hydrogenation reactions^[18]. When the Ag-Cu alloy exists in bulk form, it exhibits typical characteristics of a eutectic system. However, it is clear that still much has to be learned about these binary Ag-Cu nanoalloy particles. From the observations of in situ scanning transmission electron microscopy by Lu P et al for Ag-Cu nanoparticles, Cu and Ag atoms undergo diffusion and redistribution to form different structures^[19]. For the small-size Cu-Ag clusters, it was found that there are Cu atoms' segregations in the interior regions, and under a certain composition ratio for Cu/Ag atoms, a core-shell structure appears, which is manifested as a shell closure effect^[20]. Zhang et al. studied 38-atom Ag-Cu clusters using genetic algorithm global optimization, and found that truncated octahedral $\text{Ag}_{32}\text{Cu}_6$ is less stable than poly dodecahedral $\text{Ag}_{32}\text{Cu}_6$ core-shell clusters, where the polyhedral $\text{Ag}_{32}\text{Cu}_6$ clusters present the oxygen dissociation properties^[21]. Liu et al. found that when doping a Cu atom into different shell layers of icosahedral Ag clusters containing 55 and 147 atoms, the structural transformation of these single-atom doped clusters shows significant differences with increasing temperatures^[22], where there is a significant stress release during the structural transition with increasing temperature. For these small-size clusters, the atomic packing structures with different Cu/Ag composition ratios present significant diversities

during cooling the molten clusters. Therefore, an interesting issue arises naturally that for nanoparticles containing hundreds of atoms, how does the structural transformation during cooling the molten alloying nanoparticles with different compositions, where the information should be provided in terms of the microscopic dynamical motion of the atoms.

Accounting for the fact that nature of the transformation determined by experiment is hardly possible, computer simulations based on empirical potentials, such as molecular dynamics (MD), are particularly well suited to characterize microscopic details in these systems involving combined behaviors of atoms. Knowledge of the microscopic processes is essential for understanding the time evolution of a system by integrating classical equations of motion using the defined interactions between constituent atoms, and the measurement of these functions is very straightforward in that they are computed directly from the positions and velocities of the atoms in these particles. Successful examples of MD simulations within the framework of the embedded atom method have been performed to investigate the structural changes related to melting, freezing, coalescence, and compression of pure metal clusters or bulk, which most of them have FCC or HCP structures in their bulk phases.

In this paper, we present molecular dynamics simulations for Ag_mCu_n ($m+n=561$) nanoparticles, and the variations of local structures are demonstrated by “phase diagram” as well as atomic packing images within the embedded atom method (EAM) framework. In addition, pair distribution functions, potential energy, and entropy are also investigated and analyzed.

2. Models and Methods

In the present simulations, the interaction among the atoms is described by the EAM form, which was proposed by Williams^[23]. In this formalism, the total potential energy of the system E_{tot} is composed of $V_{ij}(r_{ij})$ and $F_i(\bar{\rho}_i)$, which respectively denote the interaction energy between atoms of i and j at a separation distance r_{ij} and the embedding energy of the electron density ρ_i at atomic position i .

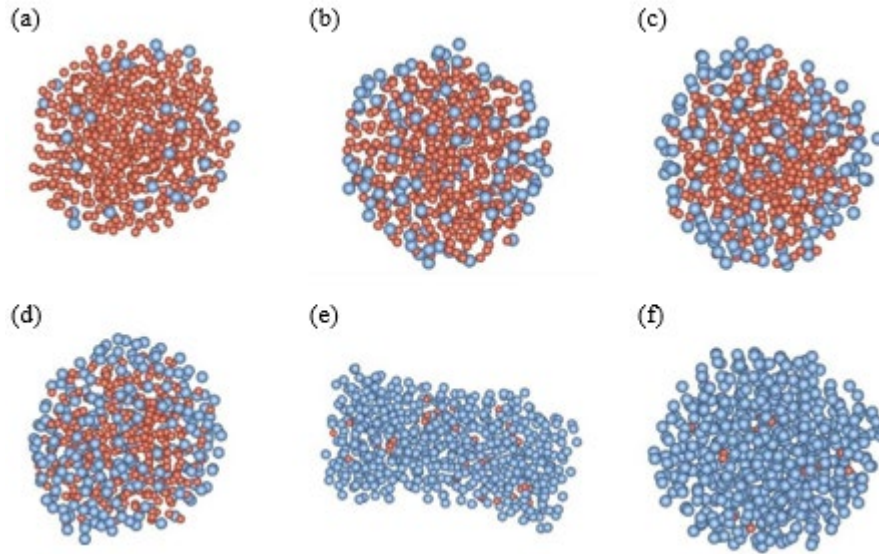
$$E_{tot} = \frac{1}{2} \sum_{ij} V_{ij}(r_{ij}) + \sum_i F_i(\bar{\rho}_i) \quad (1)$$

$$\bar{\rho}_i = \sum_{j \neq i} \rho_j(r_{ij}) \quad (2)$$

where $\rho_j(r_{ij})$ is the electron density of the neighboring atom j of atom i .

The simulations were carried out in the NVT ensemble using an Andersen thermostat. We use a predictor–corrector algorithm to obtain the positions and velocities of each atom through integrating Newton’s equations of motion. A time step of 1.6fs is used throughout the simulations. At each temperature, the system is initially equilibrated in 1.592 ns. The subsequent 8×10^{-3} ns, corresponding to the last 5000 time steps in the simulations were used to obtain thermodynamic equilibrium values, which should be larger than $3N^{-6}$, where N is the total number of atoms in the cluster. The average energy can be obtained from the sum of the potential energy which is divided by the last 5000 time steps. The increase of the statistical time will lead to the distortion of the shape of the calculated particle from average coordinates owing to the rotation of the cluster. Thus, at each temperature, we determine the packing configuration with the lowest energy in the last 5000 time steps.

Initially, a MD simulation cell with $20a_0 \times 20a_0 \times 20a_0$ (the Ag lattice constant a_0 is 4.09 Å) is constructed. One particle containing 561 atoms was extracted from the Ag bulk crystal, and then it is put in the center of one vacuum cell having the size of $20a_0 \times 20a_0 \times 20a_0$. Here, the box size of the simulated central cell is large enough to avoid the interaction of the atoms in this central cell with the other atoms in its 26 neighboring imaging cells under periodic boundary conditions. At the temperature of 1300 K, the particle would be definitively subjected to structural relaxation to obtain a molten state. In the molten cluster, five Ag atoms were replaced by the same number of Cu atoms at a time to get the newly particles. For the constructed alloying nanoparticles, the structural relaxation was performed again at 1300 K. Then, the alloyed particles in the molten state will be used for the following cooling processes. Fig. 1 shows the packing structures of molten $Ag_{36}Cu_{525}$, $Ag_{126}Cu_{435}$, $Ag_{151}Cu_{410}$, $Ag_{251}Cu_{310}$, $Ag_{521}Cu_{40}$ and $Ag_{541}Cu_{20}$ particles after structural relaxation at 1300 K, where the silvery grey balls represent Ag atoms and the red balls Cu atoms. We could see that all Ag-Cu particles were in molten states, and the atoms were all disordered at 1300K. As shown in this figure, when the particles are in disordered states, most of the Ag atoms are distributed in the outer layer of the particle, wrapping the Cu atoms inside. The $Ag_{521}Cu_{40}$ particle has an elongated shape, whereas the others have quasi sphere geometries.



(a) $Ag_{36}Cu_{525}$, (b) $Ag_{126}Cu_{435}$, (c) $Ag_{151}Cu_{410}$, (d) $Ag_{251}Cu_{310}$, (e) $Ag_{521}Cu_{40}$, (f) $Ag_{541}Cu_{20}$

Figure 1: The initial atomic packing structure of the cluster after structural relaxation at 1300K

The cooling simulations were performed by starting at 1300 K, and then decreasing the temperature to 300 K at a decrement of 50 K. The initial structures at temperatures below 1250 K were from the coordinates of the last time step of the previous temperature. By using this cooling strategy, our time scale is sufficient to produce significantly structural changes owing to the structural heredity between two temperatures.

Pair distribution function $g(r)$ gives the possibility of finding a pair of atoms which are separated by a given distance r when the atoms are randomly distributed with the same atomic density, which is given by

$$g(r) = \frac{1}{N^2} \langle \sum_{i \in N} \sum_{j \neq i \in N} \delta(r - r_{ij}) \rangle \quad (3)$$

where $\langle \cdot \rangle$ denotes the average over statistical time steps over the entire trajectory and N is the number of atoms in the cell contained within the simulated system. δ is the Dirac notation, when $r \neq r_{ij}$, δ is 1, and $r = r_{ij}$, it is zero.

The spatial distribution of the atoms of each component in one particle can be reflected by the moment of inertia, and its tensor form is as follows:

$$I_{ij} = \sum_{iatom=1}^N \left[\frac{m_{Cu}}{Ag} \times (x_{iatom}^i - x_c) \times (x_{iatom}^j - x_c) \right] \quad (i \text{ or } j = 1,2,3) \quad (4)$$

$$X_c = \sum_{iatom}^N \left(\frac{m_{Cu}}{Ag} \times x_{iatom}^i \right) / \sum_{iatom}^N \frac{m_{Cu}}{Ag} \quad (i = 1,2,3) \quad (5)$$

Among them, $m_{Cu/Ag}^i$ is the mass of Cu atom or Ag atom, x_c is the center of mass coordinate, x_i or x_j is the coordinate of atom i or j , and 1,2, and 3 correspond to the x , y , and z axes, respectively. Three values of I^1 , I^2 , and I^3 are obtained by diagonalizing the tensor components, where I^1 and I^3 are the maximum and minimum values on the main diagonal of the moment of inertia, respectively. The shape factor can be obtained by:

$$K_{shape} = I^1 / I^3 \quad (6)$$

The shape factor is a number which is always greater than 1, and if the shape factor value is closer to 1, the cluster would have an approximately spherical shape.

To describe the degree of disorder in a system, entropy S can be defined as:

$$S = \frac{E_{\text{tot}} - F}{T} \quad (7)$$

In the formula, E_{tot} is the total potential energy, F is the free energy of the system, and T is the temperature. The free energy consists of the translational free energy F_t and the rotational free energy F_r , which can be described as:

$$F = F_t + F_r \quad (8)$$

F_t is obtained from the following formula:

$$F_t = -k_B T \times \ln Z_t \quad (9)$$

where k_B is the Boltzmann constant, and Z_t is the translational partition function, which is determined by the temperature. The rotational free energy can be given by:

$$F_r = -k_B T \times \ln Z_r \quad (10)$$

Here, the rotational partition function Z_r is determined by the spatial distribution of the atoms of each component in the cluster.

3. Results and discussion

Fig. 2. shows the structural diagram of the particles $\text{Ag}_{561-n}\text{Cu}_n$ ($n=1-561$) during the cooling of the nanoalloys from 1300 K to 300 K. Here, we use Ih to denote the icosahedral configuration, Ih' the elliptical ring structure, α FCC packing of Ag atoms, β FCC packing of Cu atoms, α' the coexistence of partially FCC and partially disordered structures, and γ the coexistence of partially icosahedral and partially disordered structures. As shown in this figure, when the number of Cu atoms is less than 135, the structural transition temperatures decrease in an oscillation mode accompanying with the atomic packing structure of the particles changing from disordered to ordered patterns. For the particles having Cu atoms being more than 310, the structural transition temperature increases in a similarly oscillating mode. For the two pure nanoparticles of Ag_{561} and Cu_{561} , they have similar structural transitions from disordered packing structures to FCC packing, where multiple regions of the FCC packing appear within the two particles, and there are coherent atomic layers at the interfaces of these regions. For Ag atoms' numbers between 561 and 501, i.e., particles containing a small number of Cu atoms, most of the alloy particles also exhibit a α "twin" structure at low temperatures as shown on the left side of the diagram. Only when 5 and 15 silver atoms are replaced by copper atoms, the alloying particles show an icosahedral packing configuration. Similar images occur when the number of Ag atoms in the particles is very small, resulting in a "quintuple twin" packing pattern as in the case of $\text{Ag}_1\text{Cu}_{560}$ particles, where the structural transition temperature is significantly higher than that of an alloy particle having a larger number of silver atoms. For Ag atoms' numbers ranging from 101 to 1, most of the particles exhibit Ih geometry, while some of them still exhibit β -type packing. At the number of Ag atoms contained in the particles within 521, the particles also exhibit an elliptical ring structure (Ih'). As more Ag atoms are replaced by Cu atoms, the particles containing 506 to 461 Ag atoms present a transform to γ -type structure with icosahedral packing, and as the temperature decreases, multiple structures coexist. Here, FCC packing coexists with other packing structures in some regions within the alloy particles containing 491 and 476 Ag atoms. For these particles having Ih geometries, the silver atoms are more uniformly distributed in different regions of the particles, whereas the copper atoms are mainly distributed in the interior regions. A similar phenomenon occurs in the incomplete α structure, where the silver atoms are arranged in a more orderly manner, but an incomplete icosahedral structure appears inside the particle, while the copper atoms are in the core of the particle. When the number of silver atoms within the particle decreases below 456, there is no longer a significant disorder-order packing transition temperature in the particles. In these particles, Ag atoms are disorderly arranged in the outer parts, and most of the Cu atoms appear in the center of the particles. For the alloy nanoparticles containing more than 251 silver atoms, a major majority of the atoms in the particles are disordered with decreasing the temperature. A small number of the particles still present the Ih packing configurations. When the number of Ag atoms decreases below 251, the clusters at low temperatures start to exhibit icosahedral features. In them, as the number of copper atoms increases, the ordered icosahedral phenomenon becomes more pronounced, and with increasing the number of copper atoms, the particles with Ih and FCC configurations appear.

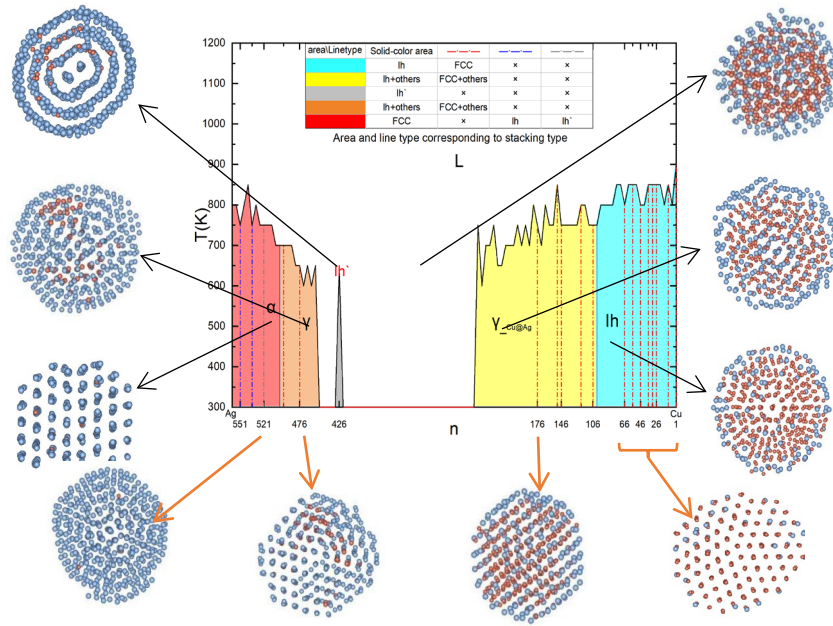


Figure 2: Structure diagram of Ag_nCu_{561-n} ($n=561-0$) nanoalloys

Fig. 3 shows pair-distribution functions (PDFs) of six alloying particles including $Ag_{541}Cu_{20}$, $Ag_{521}Cu_{40}$, $Ag_{251}Cu_{310}$, $Ag_{151}Cu_{410}$, $Ag_{126}Cu_{435}$, and $Ag_{36}Cu_{521}$ at room temperature, where the six particles have α , α' , β , γ , Ih and Ih' as shown in the above structure diagram or “phase diagram”. In the PDFs, discrete peaks indicate the ordering of the packing structure of the atoms. It should be noted that the first peak of these PDFs is higher than the other peaks, suggesting that most of atoms’ pairs are populated within the distance corresponding to the position of the first peak. The PDFs of Ih and Ih' structures present differences in their peak’s positions and shapes. For the α packing structure, the first main peak corresponding to the first nearest neighboring atoms have the largest spacing than those in the other structures. In addition, the shape of the first main peak of the core-shell Ih does not exhibit a symmetrical form, which is due to the small differences in the distances among the atoms’ pairs forming between Cu-Cu, Cu-Ag, and Ag-Ag atoms. The γ packing structure has several broadened peaks and the PDF curve is relatively flat, suggesting the locally disordered packing.

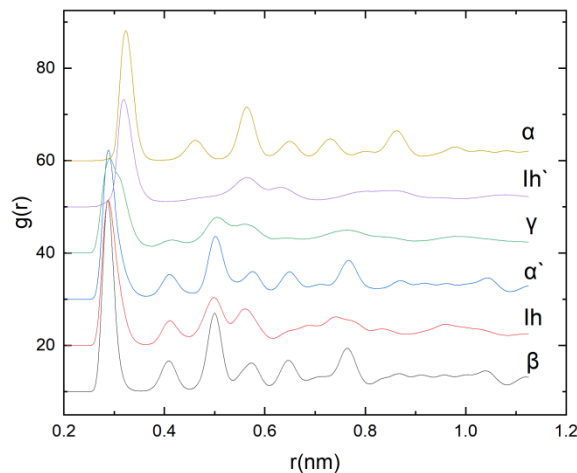


Figure 3: Paired distribution functions (PDF) for six packing structures.

With replacing the Ag atoms by different numbers of the Cu atoms, the electron densities in different regions are different, resulting in differences both of the interaction energy of atom pairs and the embedding energy of the atoms contribute to the total potential energy. As the temperature changes, the distances among the atoms’ pairs also changes. Correspondingly, the energy changes too. Therefore, the atomic energy and shape can be used to present the differences in composition and structures in these

clusters. Fig. 3 illustrates the variations of potential energy per atom and shape factor as a function of the temperature for six alloying particles. The potential energy of each of the six packing patterns decreases continuously as the temperature decreases. As illustrated in this Fig.4(a), the atomic energy of the Cu-Ag alloying particles decreases with the increase of the number of Cu atoms, suggesting that the substitution of the Cu atoms for the Ag atoms is beneficial to the stability of the alloying nanoparticles. For $\text{Ag}_{541}\text{Cu}_{20}$ and $\text{Ag}_{521}\text{Cu}_{40}$, the components are similar, and therefore the curves are closer together. For the former, the energy drops abruptly between 850 K and 800 K, which indicates a significant change in the structure of the particle from disordered packing to an α type. Further calculations indicate a crystallization temperature of 802 K through a binary algorithm. As the temperature decreases below 800 K, the potential energy decreases linearly with temperature. From the change in shape factor during cooling as shown in Fig.4(b), we can find that the shape factor of the $\text{Ag}_{541}\text{Cu}_{20}$ reaches 2.82 at 1150 K, indicating that the particle is significantly elongated. Afterwards, the shape of this particle keep this rod-like shape. Below 850 K, the atoms in this cluster present FCC packing patterns. For $\text{Ag}_{521}\text{Cu}_{40}$, the cluster structure is transformed from disordered to Ih' at a temperature of 781 K. After that, the cluster energy decreases uniformly and slowly as the temperature decreases. This indicates that the $\text{Ag}_{521}\text{Cu}_{40}$ cluster is always elongated in the temperature interval from 1300 K to 300 K. The potential energy of the $\text{Ag}_{251}\text{Cu}_{310}$ particle is significantly lower those of the above two particles, and below 750K, the particle has a γ' packing. It can be noted from the shape factors that this particle can hold its nearly spherical shape during the cooling process. For the $\text{Ag}_{151}\text{Cu}_{410}$ particle, between 900 K and 800K, there is a decrease stage of the atomic energy in a bigger slope than those above 950K and below 750K. When the Ag atoms' number decreases to 126, the particle's potential energy decreases in the temperature range 1200 K to 800 K, and then a significant decrease occurs from 800K to 750K, indicating that a locally ordered transition occurs. The change in potential energy of the $\text{Ag}_{36}\text{Cu}_{525}$ particle shows that it change from disordered to β -structure in the range of 900 K to 850 K. For the four particles, their shape factors are always slightly larger than one during cooling, indicating that they have the spherical shape.

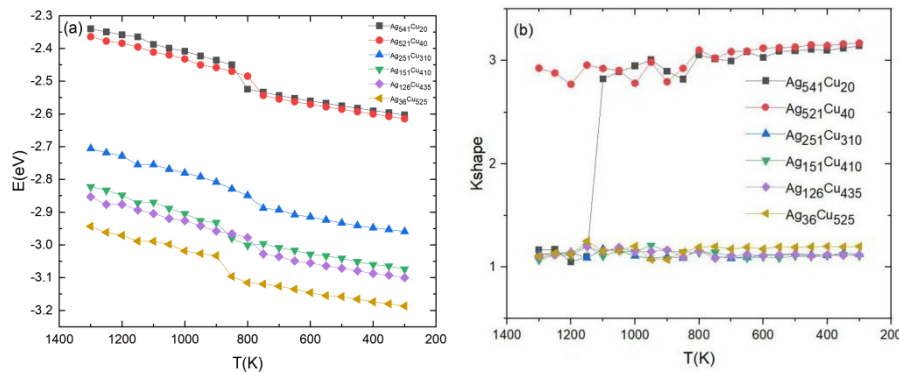


Figure 4: Variation in the potential energy per atom and shape factors of the six particles. (a) Potential energy; (b) Shape factor

Fig. 5 shows the packing images of the $\text{Ag}_{541}\text{Cu}_{20}$, $\text{Ag}_{521}\text{Cu}_{40}$, $\text{Ag}_{251}\text{Cu}_{310}$, $\text{Ag}_{151}\text{Cu}_{410}$, $\text{Ag}_{126}\text{Cu}_{435}$, and $\text{Ag}_{36}\text{Cu}_{525}$ particles at different temperatures. From the views of different directions for the $\text{Ag}_{541}\text{Cu}_{20}$ particle, we can find that at 1200K, the atoms pack disorderly, where the Cu atoms locate randomly at different positions of this particle. It can be noted that this particle has a cylindrical shape. As the temperature decreases to 850 K, many atoms are packed orderly, and the whole particle presents a laminar arrangement. At 300K, most of them are packed in FCC patterns, where the atoms in the interface have HCP packing. At 1200K, the $\text{Ag}_{521}\text{Cu}_{40}$ particle has a spherical geometry. With decreasing the temperature to 800 K, this rod particle present four-layers rings in its cross-section, and then it presents an elliptical cross-section. As the temperature decreases, many atoms are packed orderly. For the $\text{Ag}_{251}\text{Cu}_{310}$ particle, at 1200K, most of the Cu atoms gather at the core of this particle. In the following temperature regime, when this particle holds the Cu core/Ag shell morphology, some atoms are packed in Ih structures. During cooling the $\text{Ag}_{151}\text{Cu}_{410}$ particle, the particle has a α' configuration, where some atoms in the periphery are still disordered. At 300 K, most atoms are packed in FCC patterns. The $\text{Ag}_{126}\text{Cu}_{435}$ particle is in disordered states above 800 K, and then it transforms into an icosahedral (Ih) structure when the temperature drops below 800 K. Here, the Ag atoms wrap around the Cu atoms to form a shell. At 300 K, the silver atoms are also gradually distributed evenly in the shell accompanying with interchange position among some Cu and Ag atoms. For the $\text{Ag}_{36}\text{Cu}_{525}$ cluster, it transforms from a disordered structure to a "quintuple twin" structure at 850 K, where the packing patterns in different regions is face-centered cubic. As the temperature decreases, the atomic packing remaining the α pattern,

where the atoms are packed orderly.

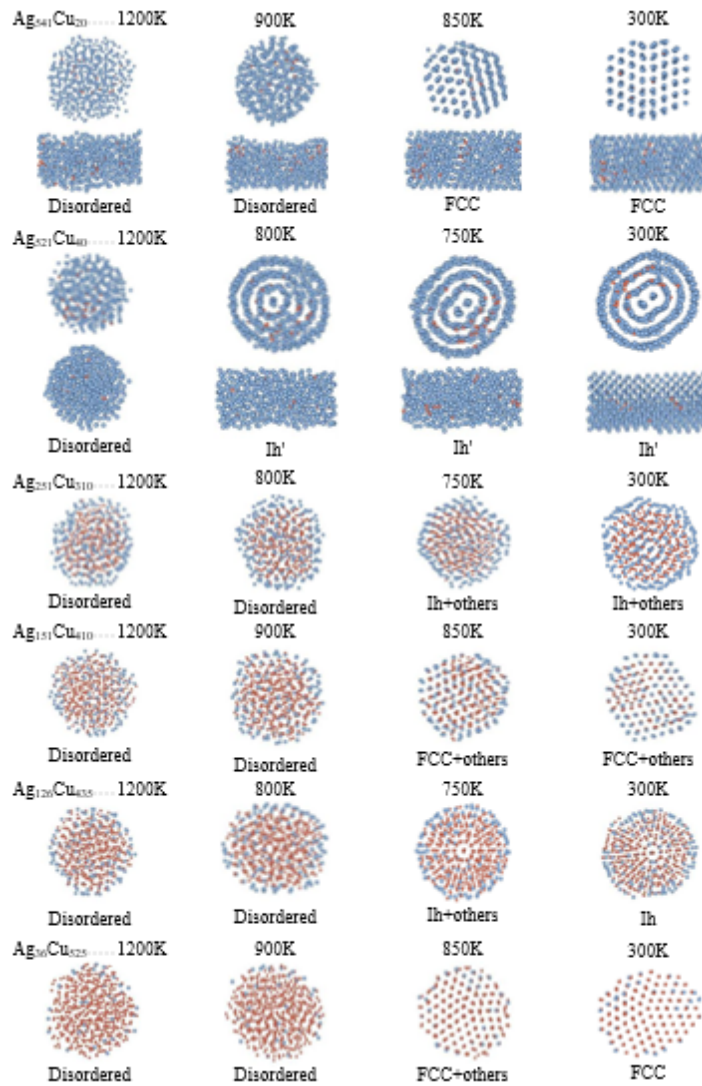


Figure 5: Stacking structure of clusters at different temperatures

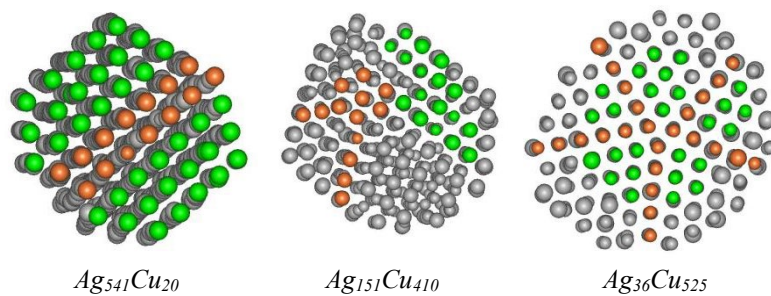


Figure 6: Packing structures of three particles including $Ag_{541}Cu_{20}$, $Ag_{151}Cu_{410}$, and $Ag_{36}Cu_{525}$ at room temperatures.

The cross-sectional images of the three particles including $Ag_{541}Cu_{20}$, $Ag_{151}Cu_{410}$, and $Ag_{36}Cu_{525}$ at 300 K is shown in Fig. 6. Here some interfacial atoms among different regions within the particles are shown with red balls, the FCC packing atoms with green ones, and the atoms having the other patterns are in gray. For the $Ag_{541}Cu_{20}$, the atom packing presents a regular symmetric twin, where the interfacial atoms are packed in HCP. The $Ag_{151}Cu_{410}$ particle consists of many local structures including FCC and HCP as well as other packing patterns, where the regions are not symmetrically arranged. In the $Ag_{36}Cu_{525}$ particle, most atoms are packed in FCC patterns, and these atoms at the coherent lattice positions are HCP packing. It can be noted that this particle can be viewed as five regions, forming quintuple twins.

Fig. 7 illustrates the change of entropy of the six particles during the cooling process from 1300 K to 300 K. As illustrated in this figure, the entropy first decreases slowly as the temperature decreases, and then decreases rapidly to negative values, and the rate of decrease gradually increases with decreasing temperature. Among the six particles, we can see that the $\text{Ag}_{521}\text{Cu}_{40}$ has the highest entropy value among them, followed by $\text{Ag}_{541}\text{Cu}_{20}$, $\text{Ag}_{251}\text{Cu}_{310}$, $\text{Ag}_{151}\text{Cu}_{410}$, $\text{Ag}_{126}\text{Cu}_{435}$, and $\text{Ag}_{36}\text{Cu}_{525}$ particles. For these five particles, as the Cu atoms' number increases, the entropy decreases. Although the $\text{Ag}_{541}\text{Cu}_{20}$ and $\text{Ag}_{521}\text{Cu}_{40}$ particles have similar rod shapes in relatively low temperature regime, the entropy of the $\text{Ag}_{521}\text{Cu}_{40}$ is significantly higher than that of the $\text{Ag}_{541}\text{Cu}_{20}$ as well as the other four particles. From the packing images at different temperatures, we can find that the $\text{Ag}_{541}\text{Cu}_{20}$ present more orderly FCC packing patterns than those of the $\text{Ag}_{521}\text{Cu}_{40}$.

We can get the implication that the number of replaced Cu atoms in the particles has a significant effect on the entropy value of the cluster.

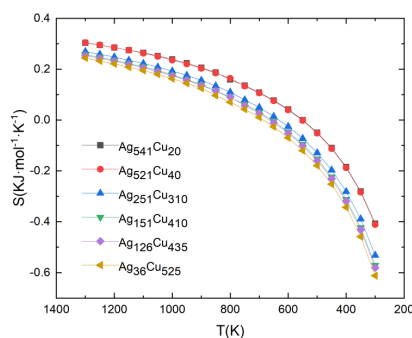


Figure 7: Entropy curves of the six clusters with temperature

4. Conclusion

We have performed molecular dynamics simulations for the structural changes as well as related entropy of $\text{Ag}_n\text{Cu}_{561-n}$ (n takes an integer between 0 and 561) nanoalloy particles during the cooling process from 1300 K to 300 K. The alloy nanoparticles in molten states have rod or spherical shapes. As the temperature decreases, the shape changes from spherical shape to rod can occur. As the Cu atoms increases, the particles exhibit different transition paths and various packing patterns. For the Ag-rich or Cu-rich alloying nanoparticles, structural transition temperatures can be identified from disordered modes to FCC or Ih packing, whereas most of the other nanoparticles with different Cu/Ag composition ratios present relatively continuous structure changes on cooling. Here, Cu core- Ag shell packing patterns can be found in Cu-rich regime. Replacing the Ag atoms with the Cu atoms is beneficial to the stability of the alloying nanoparticles in the Cu-rich regime, where the Cu and Ag atoms do not mix randomly due to the fact that the clusters tend to undergo stably alloying in energetically favorable structural configurations. Alloy compositions as well as the degree of orderly packing have significant effect on the entropy of the nanoalloys. Accompanying with the entropic decrease, the stable packing structures of the clusters are most likely to appear in the temperature range in which the freezing nanoparticles, and some packing patterns are stable.

Acknowledgement

This work was supported by the GHfund B(202302026626)

References

- [1] Novak J P, Brousseau L C, Vance F W, et al. Nonlinear Optical Properties of Molecularly Bridged Gold Nanoparticle Arrays [J]. *Journal of the American Chemical Society*, 2015, 122(48):12029-12030.
- [2] Cho U R, Kai W, Kim G W, et al. Effects of Ag Seed on Synthesis of FeCo Nano-Particles Prepared via the Polyol Method [J]. *Journal of Materials Science and Technology -Shenyang-*, 2010, 26(7):660-

664.

- [3] Lu L Y, Yu L N, Xu X G, et al. Monodisperse magnetic metallic nanoparticles: synthesis, performance enhancement, and advanced applications[J]. *ChemInform*, 2013, 45(4):323-331.
- [4] Perla V, Ejiofor J U, Webster T J, et al. Directed osteoblast adhesion at particle boundaries: promises for nanophase metals[J]. *Biological and Bioinspired Materials and Devices*, 2004, 823:207-212.
- [5] Haik Y, Chatterjee J, Chen C J, et al. Synthesis and stabilization of Fe-Nd-B nanoparticles for biomedical applications *Journal of Nanoparticle Research*, 2005, 7(6), 675-679.
- [6] Sun J, Chen M, Cao G, et al. The effect of nano-hydroxyapatite on the microstructure and properties of Mg-3Zn-0.5Zr alloy[J]. *Journal of Composite Materials*, 2014, 48(7).
- [7] Luo J, Yin J, Loukrakpam R, et al. Design and electrochemical characterization of ternary alloy electrocatalysts for oxygen reduction reaction[J]. *Journal of Electroanalytical Chemistry*, 2013, 688: 196-206.
- [8] Mueller C M, Murthy R R, Bourgeois M R, et al. Thermodynamic Determination of Bimetallic Particle Geometry: Suitability of Poorly Miscible Alloys for Surface Enhanced Raman[J]. *The Journal of Physical Chemistry C*, 2020, 124(5), pp.3287-3296.
- [9] M Jahnatek, O Levy, GLW Hart, et al. Ordered phases in ruthenium binary alloys from high-throughput first-principles calculations [J]. *Physical review*, 2011, 84(21):p. 214110. 1-214110. 8.
- [10] Chiba M, Thanh M N, Hasegawa Y, et al. Synthesis of binary solid solution Cu-Pd nanoparticles by DMF reduction for enhanced photoluminescence properties [J]. *Journal of Materials Chemistry C*, 2014, 3(3):514-520.
- [11] Jiang S, Ma Y, Tao H, et al. Highly Dispersed Pt-Ni Nanoparticles on Nitrogen-Doped Carbon Nanotubes for Application in Direct Methanol Fuel Cells[J]. *Journal of Nanoscience and Nanotechnology*, 2010.
- [12] Noh S H, Han B and Ohsaka T. First-principles computational study of highly stable and active ternary PtCuNi nanocatalyst for oxygen reduction reaction[J]. *Nano Research*, 2015. 8(10), 3394-3403.
- [13] Sun J, Ma H F, Gao F. General synthesis of binary PtM and ternary PtM1M2 alloy nanoparticles on graphene as advanced electrocatalysts for methanol oxidation [J]. *Journal of Materials Chemistry A*, 2021, 3(31), 15882-15888.
- [14] Bhanage B M, Bhosale M A. Silver Nanoparticles: Synthesis, Characterization and their Application as a Sustainable Catalyst for Organic Transformations[J]. *Current Organic Chemistry*, 2015, 19(8)
- [15] Hiroaki, Tatsumi, Yusuke, et al. Sintering Mechanism of Composite Ag Nanoparticles and its Application to Bonding Process Effects of Ag₂CO₃ Contents on Bondability[J]. *Preprints of the National Meeting of JWS*, 2007 f:356-356.
- [16] Yaxiong C, Xihaizhu D. Enhanced Photocatalytic Efficiency of TiO₂ by Combining the Modification of Ag Nanoparticles with the Application of Anodic Bias[J]. *China Chemical Express:English*, 2003, 14(5):539-542
- [17] Dai Min. Preparation and catalytic properties of bimetallic nanomaterials[D]. Nanjing University, 2014.
- [18] Gawande, Manoj B., Goswami, Anandarup, Felpin, Francois-Xavier, Asefa, Tewodros, Huang, Xiaoxi, Silva, Rafael. & Varma, Rajender S. Cu and Cu-Based Nanoparticles: Synthesis and Applications in Review Catalysis. *Chemical Reviews*, 2016(6).
- [19] Lu P, Chandross M, Boyle T J, et al. Equilibrium Cu-Ag nanoalloy structure formation revealed by in situ scanning transmission electron microscopy heating experiments[J]. *APL Materials*, 2014, 2(2):1-980.
- [20] W. Z. Li, L. Kuai, Q. Qin and B. Y Geng, Ag-Au bimetallic nanostructures: Co-reduction synthesis and their component-dependent performance for enzyme-free H₂O₂ sensing, [J]. *Mater. Chem. A*, 2013, 1, 7111.
- [21] Zhang N, Chen F Y, Wu X Q. Global optimization and oxygen dissociation on polyicosahedral Ag₃₂Cu₆ core-shell cluster for alkaline fuel cells[J]. *Rep*, 2015, 5(1):11984.
- [22] Liu Jinhan. Atomic simulation of melting and condensation of Ag nanoclusters [D]. Northeastern University, 2019. DOI: 10.27007/d.cnki.gdbeu.2019.001051.
- [23] Williams P L, Mishin Y, Hamilton J C. An embedded-atom potential for the Cu - Ag system[J]. *Modelling & Simulation in Materials Science & Engineering*, 2006, 14(5):817.